공학석사학위논문

로켓 노즐용 고강도 내열금속 소재의 삭마 현상에 대한 연구

Study on the Ablation Phenomenon of High-Strength Refractory Metal for Rocket Nozzle Throat

2015년 2월

서울대학교 대학원

기계항공공학부

김 평 기

Abstract

Ablation experiments for pure tungsten and tungsten composites, W-HfC and W-ZrC, with addition of Computational Fluid Dynamics were performed to study the ablation characteristics and ablation resistance of the materials. Ablation characteristics of pure tungsten with respect to enthalpy and stagnation pressure were studied through series of ablation experiments. The amount of recession caused by ablation increased with respect to enthalpy and the mass lost due to ablation was found to be linearly proportional to the stagnation pressure. In addition to the experiment, ablation phenomenon analysis framework was established. Tungsten ablation was analyzed for the mentioned experiments to obtain results, such as maximum surface temperature, interior temperature distribution of the tungsten specimen, etc., which were not possible with the experiments. Moreover, to overcome the weakness of tungsten; vulnerable to oxidation and ablation in high-temperature conditions, W-ZrC and W-HfC composites were manufactured using three different methods. Ablation experiments and micro-structural analyses were carried out to study the ablation characteristics and ablation resistance of W-ZrC and W-HfC with respect to manufacturing method and volume fraction of ZrC and HfC. Methods to increase tungsten composites ablation resistance were suggested with the basis of results of the experiments, CFD analyses, and micro-structural analyses. The suggested methods were to produce composites with small particles and to form ZrO_x, HfO_x layer on the surface.

.....

Keywords : Ablation, tungsten, W-HfC, W-ZrC, ablation resistance, CFD

Student number : 2013 - 20662

Table of contents

List of figures

List of tables

1. Introduction

1.1 Background

In recent years, as the national interest and funding in space exploration increases with addition of development of research tools such as experimental devices and computing resources, the opportunities and needs for researches related to space exploration are being widened. One of the required fields of research for such growing interest is development of launch vehicles. Prior to developing launch vehicles, design techniques for appropriate rocket nozzle components including rocket nozzle shape, nozzle throat, etc., need to be acquired.

Rocket nozzle throat insert materials are exposed to a very severe thermodynamical and mechanical conditions. In order to function its purpose in such extreme conditions, nozzle throat insert materials should have high melting temperature and also be able to maintain its high mechanical properties in high-temperature conditions. In addition to the mentioned properties, materials with high moldability can be useful since it is easier to change the shape of the insert material according to the shape of the nozzle throat. The materials meeting the mentioned standards are generally categorized as refractory materials.

1.2 Refractory metal for rocket nozzle throat

Typically, rocket nozzle throat inserts are used in the temperature range from the standard room temperature to 3000 K. In such high-temperature conditions, conventional composites with their melting points around 1800 K cannot be used. Instead, Materials with higher melting points such as rhenium, platinum or metal/ceramic 3D network

structured composites. Ceramics of the composites function to support the structure of the overall composites with their great mechanical properties, and metals function to lower the temperature of the overall composites by phase changing with the absorbed heat.

The extreme conditions refractory metals for rocket nozzle throat are subjected to makes it essential to have high-strength abrasion/heat-resistance. Among many refractory materials, metals with high melting point -tungsten, titanium, zirconium, hafnium, vanadium, niobium, tantalum, chrome, molybdenum-based refractory metals are widely utilized in the fields of industrial and material science. Tungsten as refractory metal for rocket nozzle can be advantageous for its high melting point and great mechanical properties. Because of the great thermodynamical, and mechanical properties of tungsten, it is widely used for supersonic jets, gas turbine blades, high temperature gas nozzle for rockets and nuclear reactors. However, tungsten is vulnerable to oxidation when exposed to high-temperature air. In order to overcome such weakness, it is essential that ways to enhance tungsten's ablation/oxidation resistance be studied throughly.

1.3 Ablation phenomenon of tungsten

Ablation phenomenon of tungsten generally classified into 3 categories; ablation due to surface chemical reactions, ablation due to melting of tungsten oxides, and mechanical ablation due to shear erosion. The surface chemical reactions which has significant effect on ablation include sublimation, oxidation and catalytic recombination. Reactions with major impact on ablation are equated as follows.

Table 1.1 Chemical reactions with significant effect

No	Reaction
	Sublimation
1	$W(s) \leftrightarrow W(g)$
	Oxidation
2	$\frac{1}{2}O_2(g) + W(s) \leftrightarrow WO(g)$
3	$O_2(g) + W(s) \leftrightarrow WO_2(g)$
4	$\frac{3}{2}O_2(g) + W(s) \leftrightarrow WO_3(g)$
5	$3O_2(g) + 2W(s) \leftrightarrow W_2O_6(g)$
6	$O(g) + W(s) \leftrightarrow WO(g)$
7	$2O(g) + W(s) \leftrightarrow WO_2(g)$
8	$3O(g) + W(s) \leftrightarrow WO_3(g)$
9	$6O(g) + 2W(s) \leftrightarrow W_2O_6(g)$
	Catalytic recombination
10	$O(g) + O(g) \leftrightarrow O_2(g)$

The product of tungsten oxidation, WO_3(~1746 K), has a relatively low melting point compared to that of pure tungsten. Therefore, when oxidation takes place, formation of tungsten oxide on the surface of tungsten leads to formation of melt layer which is easily blown downstream of the flow. In addition, mechanical ablation occurs due to

the shear force exerted on the wall of tungsten specimen. As stated, ablation of tungsten comprises of a series of chemical reactions and physical phenomena making it a greatly challenging topic. In order to study the ablation characteristics of tungsten and suggest ways to enhance ablation resistance of tungsten, variety of experiments for pure tungsten and tungsten composites were performed with addition of Computational Fluid Dynamics(CFD) in this study.

2. Ablation experiments of pure tungsten

Ablation phenomenon in extreme conditions mentioned in Section 1 is a very complicated physical phenomenon involving a vast number of chemical reactions and many other physical phenomena. Hence, the ablation characteristics for a certain material is not very well known. For such reason, ablation characteristics of the material interested has to be acquired to throughly study the physical phenomena taking place in high-temperature conditions.

As the first step of the study presented in this study, ablation experiments for pure tungsten using plasma generator were performed. In order to achieve the experimental conditions required, a 150 kW plasma generator was used. Using the plasma generator, ablation experiments were carried out for the tungsten manufactured to be a spherical cylinder. The experiments performed in this section were categorized into 2 categories and they are as shown below table.

Table 2.1 Pure tungsten ablation experiments

No	Name	Variable	Number of conditions	Repetition	Total cases
1	Enthalpy experiment	enthalpy	3	3	9
2	Stagnation pressure experiment	stagnation pressure	3	2	6

The enthalpy experiments were performed for spherical cylinder specimens varying arc current and flow rate in order to change the required enthalpy. For a flow condition, 3 experiments were performed

varying the exposure time from 10 seconds to 30 seconds with 10 second interval. The total number of cases for the enthalpy experiments was 9. Secondly, stagnation pressure experiments were performed using the tungsten specimen shaped same as for those used in the enthalpy experiments. In order to change the stagnation pressure at the stagnation point located on the specimen, the distance from the plasma generator nozzle exit to the specimen was varied from 10 mm to 30 mm with 10 mm intervals and for each stagnation pressure, 2 repeated experiments were performed which makes the total number of experiments 6. These experiments were performed so that ablation characteristics of pure tungsten can be obtained.

2.1 150 kW plasma generator

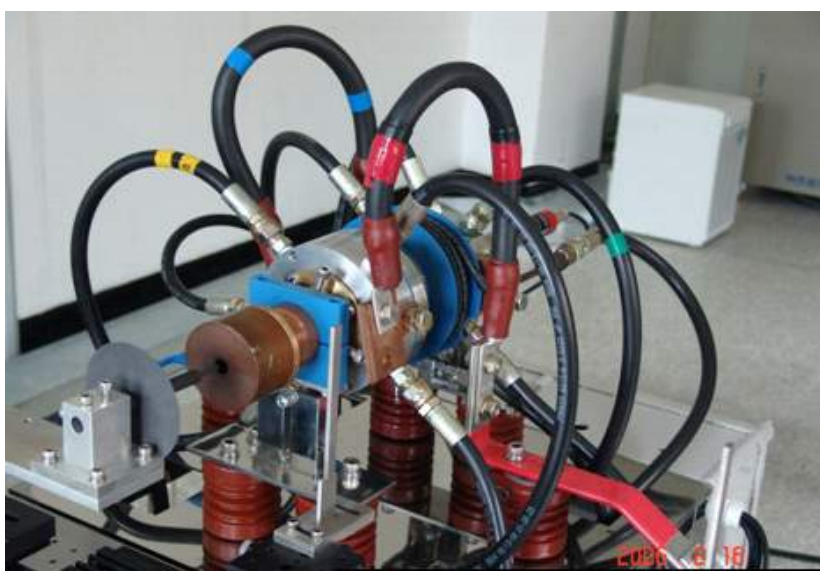

Figure 2.1 150 kW plasma generator

In order to carry out ablation experiments, a 150 kW plasma generator was used. This instrument is a enhanced Huels type which is

structurally simple and easy to maintain the performance and it can also be manufactured into a multi MW plasma generator. However, such type of plasma generator has a low value of specific enthalpy even though it can produce flow with high pressure value compared to other types of plasma generators. In addition to that, somewhat lacks in flow uniformity due to vibration generated during operation. The certain instrument used in these experiments, an enhanced Huels type, utilized constrictors to stabilize the plasma flow inside the generator. The specification of the plasma generator is as shown below.

Table 2.2 150 kW plasma generator specification

Length of the constrictor	42 mm
Diameter of the constrictor	15 mm
Diameter of nozzle throat	6~7.5 mm
Nozzle area ratio	4~7
Arc current	320~380 A
Working gas	Air
Flow rate	6~12 g/s

As mentioned in the above table, the plasma generator uses air as its working gas. The ablation experiments in this section can be illustrated as below figure.

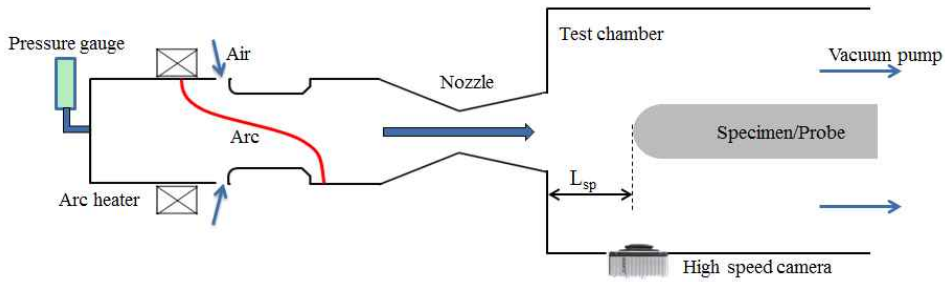

Figure 2.2 Ablation experiment schematics

High-temperature arc, shown as the red line in Figure 2.2, is generated due to the power source. Air, the working gas, is fed from the vent located in the side of the plasma generator and be heated by the generated arc to become a high-temperature, high-enthalpy plasma flow. The specimens used in these experiments were shaped to be spherical cylinders and are held by a holder made of graphite which is connected to a device which moves the holder in to the centerline of the flow and after the desired exposure time, the device moves the holder back out. The entire process of the experiments was motion captured using a high speed camera.

Figure 2.3 Pure tungsten specimen

The specimen used for the experiments were as shown in the above figure. The specimens were bright silver prior to the experiments and were shaped to be spherical cylinders with 10 mm diameter.

2.2 Enthalpy varying ablation experiments

2.2.1 Experimental conditions for enthalpy experiments

The first experiment performed to verify the ablation characteristics of pure tungsten were enthalpy experiments which were performed varying the enthalpy. These experiments were performed 9 times. The plasma flow conditions for these experiments were controlled by changing the arc current and flow rate. The arc current and flow rate conditions were 330 A and 360 A, and 9 g/s and 10 g/s, respectively. By changing the arc current and flow rate of the plasma generator, the enthalpy and pressure of the flow can be varied. The 3 flow conditions for the enthalpy experiments are as shown below in Table 2.3.

Table 2.3 Flow conditions for the enthalpy experiments

Flow condition	Enthalpy (MJ/kg)	Pressure (atm)
1	5.48	5.70
2	6.76	6.23
3	6.90	5.57

For the given flow conditions, experiments were performed 3 times each with different exposure times; 10 seconds, 30 seconds, 60 seconds, which makes the total 9 experiments. The detailed experimental conditions are as shown below.

Table 2.4 Enthalpy experiments conditions

Flow condition	No.	Arc current (A)	Arc voltage (V)	Flow rate (g/s)	Heater chamber pressure (atm)	Bulk enthalpy (MJ/kg)	Test time (s)
1	1-1	364	401	10.09	5.70	5.48	10
	1-2	364	399	10.12	5.67	5.37	30
	1-3	364	390	10.08	5.74	5.59	60
	Avg.	364	396	10.10	5.70	5.48	-
2	2-1	333	476	10.24	6.16	6.65	10
	2-2	333	476	10.10	6.16	6.65	30
	2-3	333	486	10.10	6.36	6.96	60
	Avg.	333	479	10.15	6.23	6.76	-
3	3-1	334	429	9.01	5.52	6.73	10
	3-2	334	424	9.03	5.57	6.86	30
	3-3	334	423	8.97	5.61	7.11	60
	Avg.	334	425	9.00	5.57	6.90	-

By carrying out a number of ablation experiments for pure tungsten, ablation characteristics of pure tungsten with varying enthalpy could be obtained.

2.2.2 Experimental results for enthalpy experiments

The entire process of the experiments were captured using a high speed camera. From the captured data, the shape changes for each of the 9 specimen were obtained. Each footage of the experiments were captured in 60 frames per second and the total of 600~3600 frames per experiment were captured. The captured frames show how the shape of

the specimen changes in a detailed manner. The figure shown below were chosen with 5 seconds intervals from 0 to 60 seconds for each flow condition.

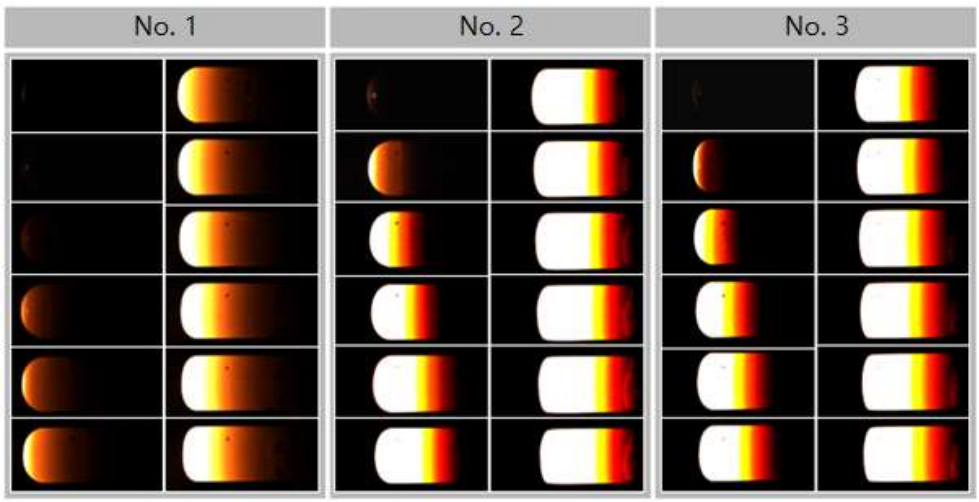

Figure 2.4 Shape change captured with high-speed camera

In the figure, the flow direction is from the left side to the right side. As can be seen from the above figure, the specimen starts to glow white as the exposure time increases. It can evidently be seen that experiment number 1 shows the darkest brightness which means that the surface temperature is the lowest, and the length change is the smallest which means that the recession amount is the smallest. On the other hand, it can be seen that experiment number 2 shows the brightest result which means that the surface temperature is the highest and also the length change is the largest which means that the amount of recession is the largest. From the experimental conditions stated above, it can be recognized that when enthalpy and pressure is low, experiment 1, surface temperature does not increase as much and recession amount is small. Contrary, if the enthalpy and pressure is high, experiment number 2,

surface temperature change and recession amount increase.

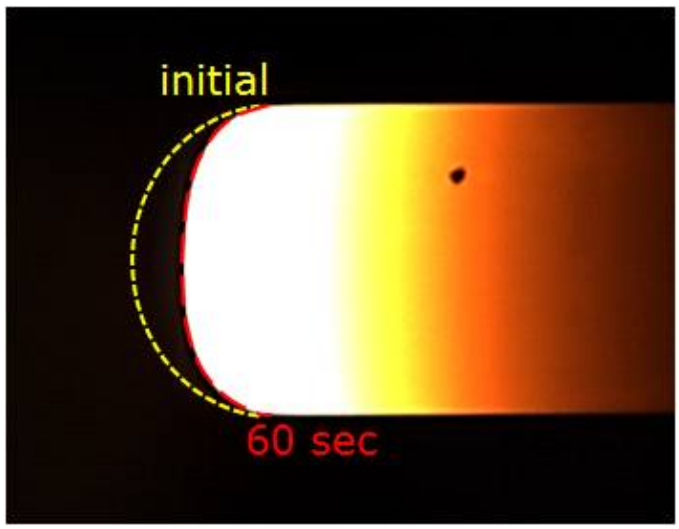

Figure 2.5 Shape change due to ablation

In addition to the temperature change characteristics mentioned above, it can also be seen that the stagnation region which was round becomes flat as recession propagates. In order to emphasize this characteristic of pure tungsten ablation, the above figure was produced. The above figure shows the initial shape in yellow dotted line and the shape after 60 seconds of exposure time in red dotted line. It can be seen that the shape after the ablation becomes significantly more flat than the initial shape of the specimen; which was fairly round. From this it can be deduced that the flow in the stagnation region is in fact laminar flow. If the flow near stagnation region is turbulent flow the heatflux drastically increase after the transition point which would be positioned downstream of the stagnation region, therefore the amount of recession at each side will be increased significantly making the shape of the front are a sharp cone or S-shaped. In this experiment, the size of the specimen is in the

order of a few millimeters which makes the Reynolds number of the flow small, hence, transition did not yet occurred. The reason being so, the effect of turbulence did not affect the ablation phenomenon. Contrary to turbulent flow mentioned above, the heatflux at the stagnation point is the greatest in laminar flow, thus the amount of recession at the stagnation point is the largest which ultimately changed the shape of the specimen to become a flat cylinder.

The post-experiment specimens of the enthalpy experiments are as shown below. The specimens in their initial state showed a bright silver color. However after the ablation experiments, the color of the specimens changed to dark blue indicating the presence of WO_3 formed on the surface due to oxidation of tungsten. Also, it was seen that yellow powder was formed at the junction between the holder and the specimen. It is thought to be the effect of relatively cold holder which made gaseous oxidized tungsten blew downstream to be re-attached. As mentioned in the above, it can be seen that the shape of the stagnation region becomes more flat from the original round shape as time propagates.

Figure 2.6 Post-experiment specimens (No. 1)

Figure 2.7 Post-experiment specimens (No. 2)

Figure 2.8 Post-experiment specimens (No. 3)

After the ablation experiments, the length at the stagnation point and the mass of the specimen were measured from which recession length data and mass loss data were obtained. The obtained data is tabulated as below.

Table 2.5 Mass loss and recession for each experiment

Condition	No.	Mass loss (g)	Recession (mm)
1	1-1	0.3	0.16
	1-2	0.6	0.63
	1-3	2.3	2.14
2	2-1	0.1	0.21
	2-2	1.8	1.69
	2-3	4.3	3.53
3	3-1	0.2	0.23
	3-2	1.6	1.37
	3-3	4.3	3.21

It indicates that the mass loss amount is the smallest for the condition

number 1 which has the smallest values of enthalpy and pressure. The mass loss after 60 seconds of the exposure time for condition 1 was measured to be 2.3 g which is about 53% of the mass loss value of 4.3 g for conditions 2 and 3. The mass loss amounts for conditions 2 and 3 were almost the same. However, the amount of recession for the conditions were slightly different. The recession amount for the condition 2 was 3.53 mm which was about 10% larger than 3.21 mm of recession for condition 3. The recession and mass loss amount for every experiments graphs were produced to be able to see the trends and are shown below.

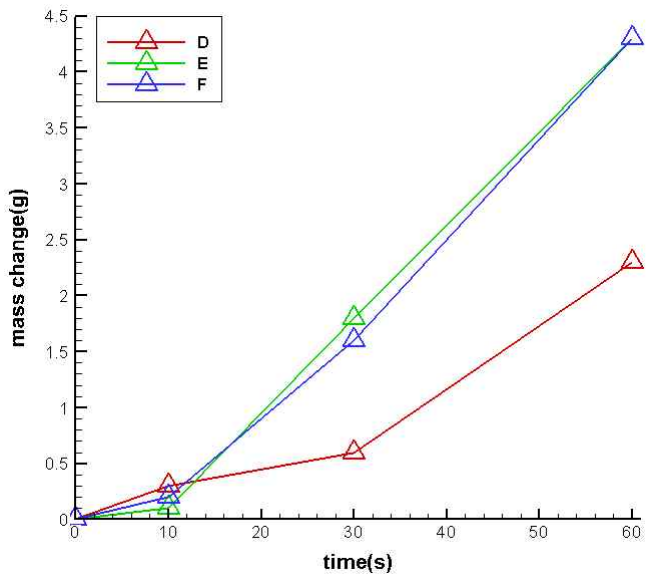

Figure 2.9 Mass loss for each experiment

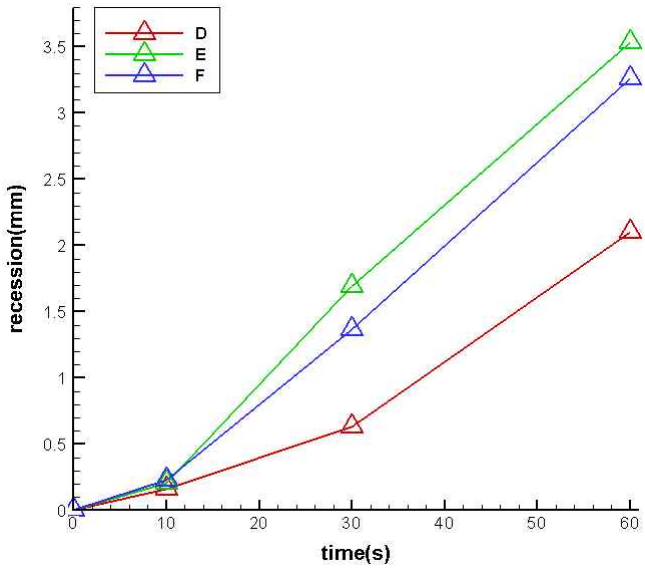

Figure 2.10 Recession for each experiment

The graphs indicate mass loss/recession amount versus exposure time; 10, 30, 60 seconds. The experimental results for conditions 1, 2, and 3 are shown as red, green, and blue line, respectively. From the graphs, it can easily be seen that enthalpy increase from condition 1 to 2 and 3 drastically increased both the mass loss and recession amount, whereas pressure change from condition 3 to 2 does not have significant effect on the amount of mass loss or recession amount. Conclusively, it was deduced that amount of recession and mass loss increases as enthalpy of the flow increases, however the pressure does not have significant effect on the amount of mass loss or recession.

The graphs shown above cannot give the exact amount of recession or mass loss if the exposure time is not 10, 30, or 60 seconds. Therefore, to obtain more accurate ablation characteristics of pure tungsten and for future research purpose, the amounts of recession due to ablation was obtained in 5 seconds intervals from the captured footage of the

experiments. The obtained stagnation point recessions for each experiment are shown below.

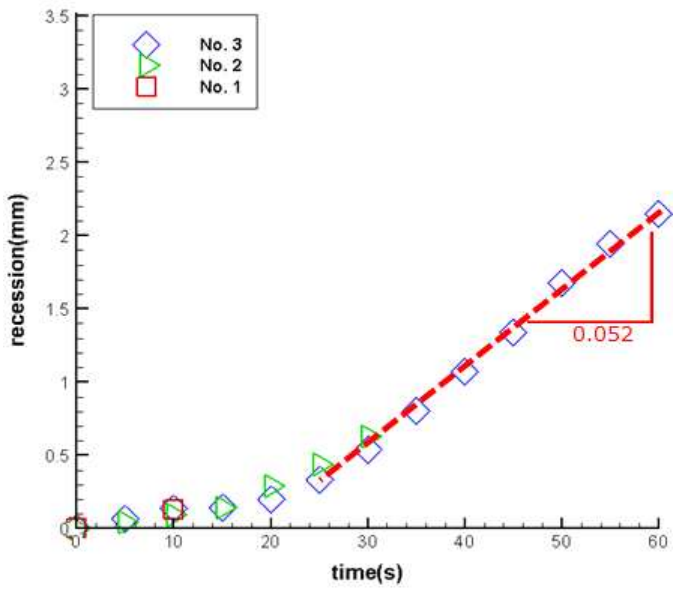

Figure 2.11 Recession vs time (condition 1)

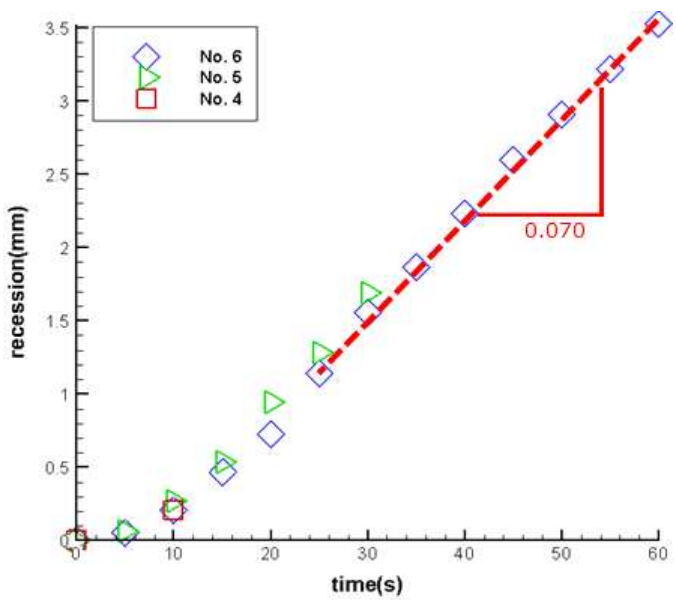

Figure 2.12 Recession vs time (condition 2)

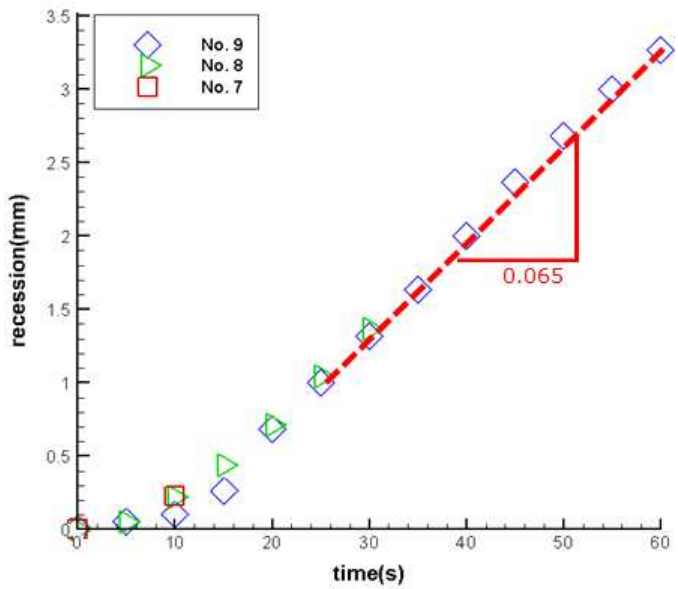

Figure 2.13 Recession vs time (condition 3)

As can be seen in the above figures, the amount of recession increases almost linearly after about 20 seconds of exposure time, from which can be deduced that the recession rate becomes at that certain moment. This steadiness of recession rate also matches with the photographic results of the experiments in which the change in brightness became minimal at about 20 seconds of the exposure time. The steady recession rates are indicated in red dotted line in the above figures and are calculated to be 0.052, 0.070, 0.065 mm/s for conditions 1, 2, and 3 respectively.

2.3 Stagnation pressure varying ablation experiments

In the previous section, the effect of enthalpy change on ablation was mainly dealt with and was shown that ablation phenomenon of pure tungsten also can be affected by the change of pressure. In order to put

emphasize on this matter and study the ablation characteristics of pure tungsten, a second set of experiments were performed; stagnation pressure experiments. These experiments were conducted to study the change in ablation phenomenon of pure tungsten with the change of stagnation pressure. The effect of pressure on pure tungsten ablation can be easily studied if the change in pressure is large enough. However, dur to the limitations of the plasma generator, the required pressure change cannot be obtained by changing the flow rate. Therefore, to vary the pressure at the stagnation point with changing least of other experimental conditions to see the effect of pressure solely, the distance from the plasma generator nozzle throat to the specimen were varied.

2.3.1 Experimental conditions for stagnation pressure experiments

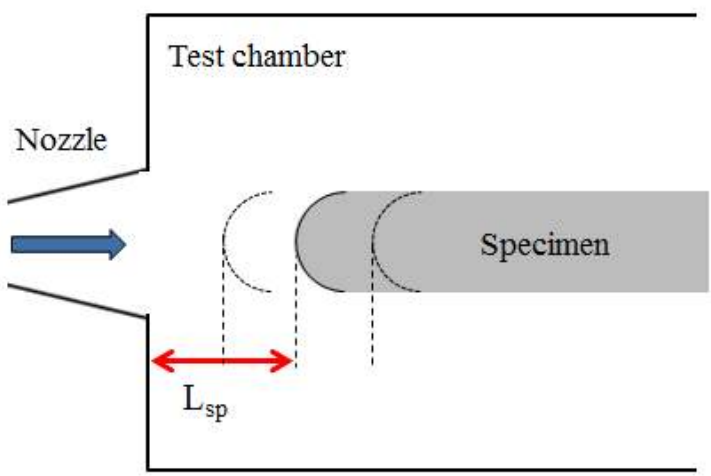

Figure 2.14 Stagnation pressure experiment illustration

The experiments were carried out for the distances of 10, 20, 30 mm from the nozzle exit to the specimen under a single flow condition for 30 seconds of exposure time. The experimental conditions for the stagnation

pressure experiments are tabulated below.

Table 2.6 Stagnation pressure experiment experimental conditions

Flow condition	Arc current (A)	Flow rate (g/s)	Chamber pressure (atm)	Enthalpy (MJ/kg)	Exposure time (s)
P1	340	12	5.64	11.383	30

As for the distances of 10~30 mm, each experiment was repeated twice making the total number of experiments 6. Distances closer than 10 mm were neglected because if the specimen was placed to close to the nozzle exit, shock wave would be formed too close to the nozzle exit resulting in a variety of highly complex physical phenomena such as flow separation, turbulence, etc. And distance further than 30 mm were also neglected since the holder moving device cannot be mobilized further.

2.3.2 Experimental results for stagnation pressure experiments

The results of the stagnation pressure experiments are tabulated in the below table.

Table 2.7 Stagnation pressure and mass loss for distances

No.	Distance(Lsp) (mm)	Stagnation pressure (kPa)	Mass loss (g)
1	30	40.46	1.6
2			1.5
3	20	56.60	2.4
4			2.5
5	10	83.33	3.4
6			3.5

Utilizing the results obtained, mass loss versus stagnation pressure graph was produced and is shown below.

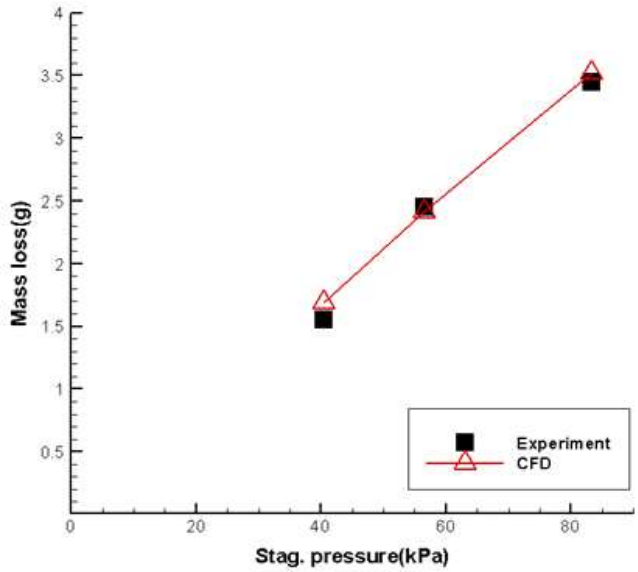

Figure 2.15 Mass loss vs stagnation pressure

As can be seen from the above table and figure, the amount of mass loss increase linearly with respect to the value of stagnation pressure. in the figure above presents Computational Fluid Dynamics(CFD) results as well as experimental results, which will be discussed later in Section 3.

3. CFD analysis of pure tungsten ablation

Performing experiments of interest is the most preferred method to obtain accurate results of ablation phenomenon occurring, but only given that the instrument and method is ready to be used. Because of extreme atmospheric conditions surrounding and the specimen itself, it is almost impossible to obtain all of the result required to study the ablation phenomenon for many materials. In order to solve this matter, computational fluid dynamics method is widely being used to study ablation and other topics involving such extreme conditions.

In this study, CFD analysis framework was settled combining a number of in-house codes and CFD analyses were conducted to obtain certain results which could not be measured for the limitations due to test facilities during the two experiments stated in Section 2. Computed results in addition to the results obtained from ablation experiments, were then utilized to study the ablation characteristics of tungsten in more detail and are discussed in following sections.

3.1 Ablation phenomenon CFD analysis framework

In order to perform an accurate CFD analysis to predict the amount of ablation, a precise flow conditions must be known. However, due to the limitations of the plasma generator test section size and lack of advanced sensors made it impossible to measure some of the flow conditions such as specimen surface temperature. The test section of the generator was too small to put thermocouples inside the specimens or other sensors around the specimens and know-hows to utilize measuring instruments and sensors in such high-temperature conditions was not

pre-occupied. Especially, the mole fraction of the air surrounding the specimen which greatly affects ablation phenomenon through series of chemical reactions could not be measured. For such reasons, framework to be used for ablation analysis was established which consists of 3 stages of calculations from which the exact values of freestream flow conditions and with the conditions, ablation was analyzed accurately. The established framework can be illustratively explained as below.

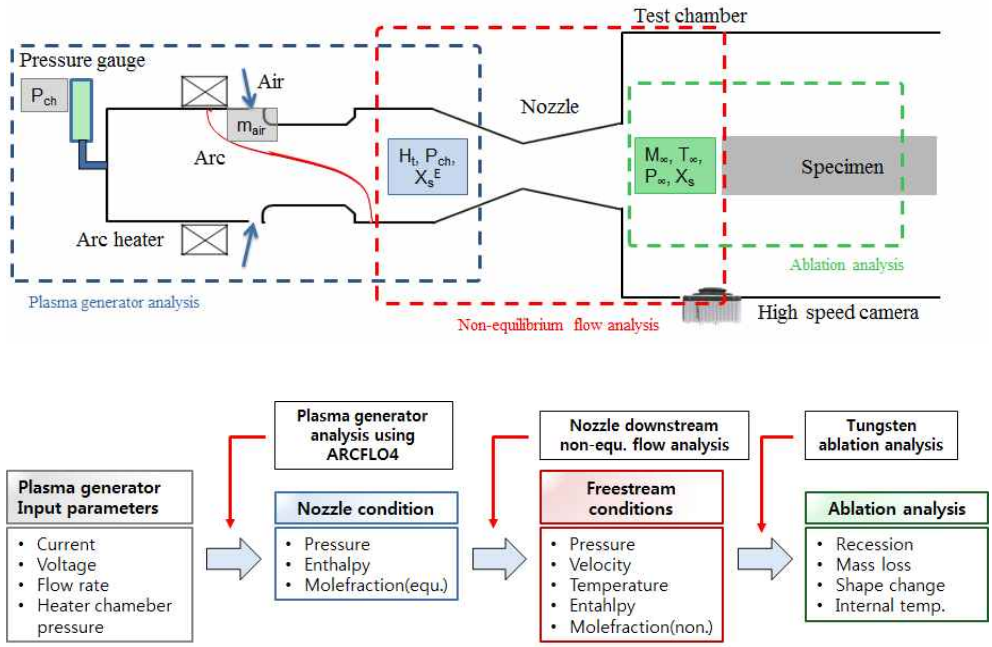

Figure 3.1 Ablation analysis framework

3.1.1 Plasma generator interior flow analysis

The region with the blue dotted line performs analysis for the plasma generator. The plasma generator uses arc current and voltage along with flow rate and heater chamber pressure as the input parameters. Flow conditions; pressure, enthalpy, and species mole fractions, at the nozzle are calculated from these input parameters through heater chamber flow analysis. At this stage of the analysis, the heater chamber pressure is

relatively high and the velocity of the flow is relatively high, therefore the flow is assumed to be in equilibrium state.

This analysis step can be done in two ways. First, using Winovich's equation, relationship between chamber pressure, enthalpy, nozzle throat area and flow rate can be obtained for a enthalpy range of 2.3~23 MJ/kg. The experiments performed has the enthalpy values all within the above range. Thus, the heater chamber enthalpy can be easily calculated using Winovich's equation as follows:

$$H_t[J/kg] = 2326 \times \left(\frac{1367 \times A^* P_{ch}}{\dot{m}_{air}} \right)^{2.5189}$$

In the above Winovich's equation, $A^*[m^2]$, and $\dot{m}_{air}$ means the nozzle throat area and air flow rate, respectively, which are known values through plasma generator input conditions and $P_{ch}[atm]$, chamber pressure which can be measured from a pressure sensor positioned near the anode of the generator. Therefore, all the values required to calculate the enthalpy can be obtained, resulting in the easily calculable value of enthalpy. In addition, the flow is assumed to be equilibrium, hence with the enthalpy and pressure known, the species molefraction can be calculated. Second method is utilizing ARCFLO4 analysis code. ARCFLO4 code takes into account electric field and radiation equations in addition with Navier-Stokes equation to calculate interior flow of plasma generators. The calculated flow conditions and species molefractions at the nozzle for the experiments performed in Section 2 are tabulated as below.

Table 3.1 Calculated flow conditions at the nozzle

No.	Experiment name	Current (A)	Voltage (V)	Chamber pressure (atm)	Flow rate (g/s)	Enthalpy (MJ/kg)
1	Enthalpy experiment	364	396	5.70	10.1	5.48
2		336	471	6.23	10.1	6.755
3		334	425	5.57	9.0	6.899
4	Stagnation pressure experiment	343	581	5.64	11.7	11.383

Table 3.2 Calculated species molefraction at the nozzle

		Species molefraction				
No.	Experiment name	O	N	NO	O_2	N_2
1	Enthalpy experiment	0.0999	0.0002	0.0648	0.1172	0.7180
2		0.1684	0.0006	0.0668	0.0746	0.6895
3		0.1788	0.0007	0.0651	0.0692	0.6862
4	Stag. pressure experiment	0.3127	0.0317	0.0279	0.0035	0.6242

3.1.2 Nozzle downstream flow condition analysis

Flow conditions downstream of the nozzle towards the specimen can be calculated through non-equilibrium flow analysis with the flow conditions at the nozzle as input parameters. Through this step, freestream flow conditions required for tungsten ablation analysis can be calculated. The freestream conditions required are pressure, temperature, Mach number, enthalpy and species molefraction. The non-equilibrium calculations were performed using the below grid system.

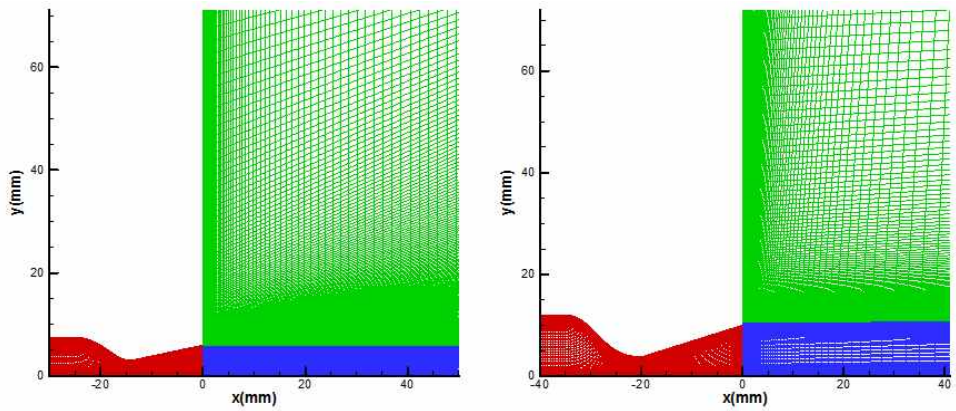

Figure 3.2 Non-equilibrium nozzle flow analysis grid system

The grid system consists of two different types as can be seen from the above figure. The enthalpy experiments and the stagnation experiments were performed using the left(Nozzle 1) and right(Nozzle 2) nozzle respectively. Each nozzle specification are as follows.

Table 3.3 Nozzle diameter and area ratio

Nozzle 1		Nozzle 2	
D*	12 mm	D*	20 mm
D_{ex}	6 mm	D_{ex}	7.5 mm
A_{ex}/A^*	4	A_{ex}/A^*	7.111

Utilizing the flow conditions calculated from the previous stage and the nozzle grid system, the non-equilibrium flow calculations can be performed. The example results (enthalpy experiment condition number 1) are presented below.

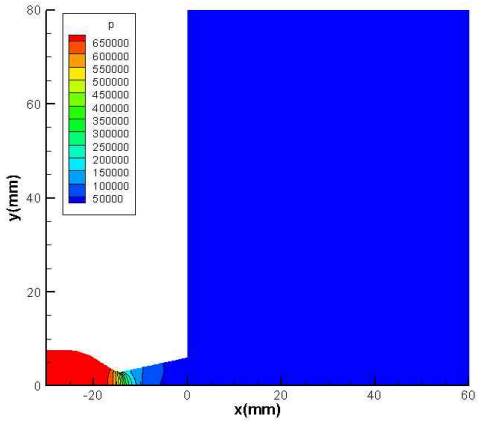

Figure 3.3 Pressure contour

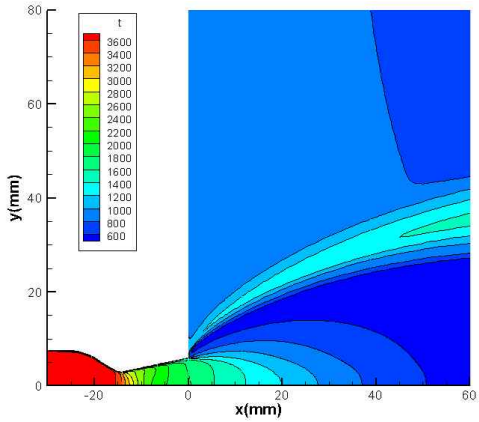

Figure 3.4 Temperature contour

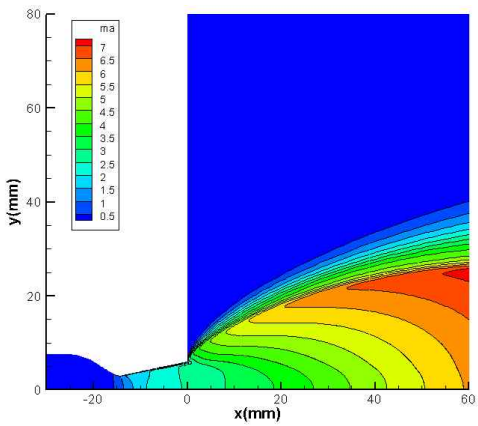

Figure 3.5 Mach number contour

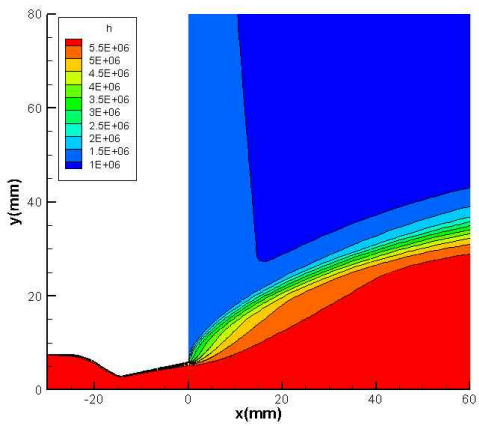

Figure 3.6 Enthalpy contour

3.2 Shape change analyses with respect to temperature

3.2.1 Shape change analyses conditions

Analysis for the shape change with respect to surface temperature were conducted using the established ablation analysis framework. The analysis was performed for the enthalpy experiments. The flow conditions and the species molefraction for these analyses are tabulated as below.

Table 3.4 Freestream conditions for shape change analysis

Flow condition	Density (kg/m^3)	Velocity (m/s)	Pressure (Pa)	Temperature (K)	Mach number	Ht (MJ/kg)
1_avg	2.61E-02	2354	11589	1468	3.01	5.5
2_avg	2.48E-02	2515	12310	1585	3.03	6.8
3_avg	2.20E-02	2526	10989	1585	3.04	6.9

Table 3.5 Species molefraction for each condition

Flow condition	O	N	O_2	N_2	NO
1_avg	3.21E-2	1.69E-7	9.98E-2	6.80E-1	3.52E-2
2_avg	5.27E-2	7.05E-7	9.23E-2	6.57E-1	3.44E-2
3_avg	5.71E-2	6.68E-7	9.15E-2	6.52E-1	3.40E-2

3.2.2 Shape change analyses results

The shape change with respect to surface temperature were analyzed using the flow conditions calculated in the previous sub-section. By carrying out the pure tungsten ablation analysis, the specimens' surface and interior temperature distribution results, which were not obtainable through ablation experiments, were obtained. The interior temperature distribution results obtained through CFD analysis can be utilized in studying the heat conduction through the tungsten specimen. In addition to the interior temperature distribution, the surface temperature distribution, especially the maximum surface temperature, plays a critical role in studying ablation characteristics of tungsten since it determines whether ceratin chemical reactions and physical phenomena takes place during ablation propagates. Detailed explanations how the analyzed results are utilized will be discussed in Section 4. The captured footage of the enthalpy experiments at the exposure time of 60 seconds were combined

with the computed pressure contour of the flow. The combined results for each flow condition numbers 1, and 2 are presented as below and show a good match between the computed results and the experimental results of the shape changes.

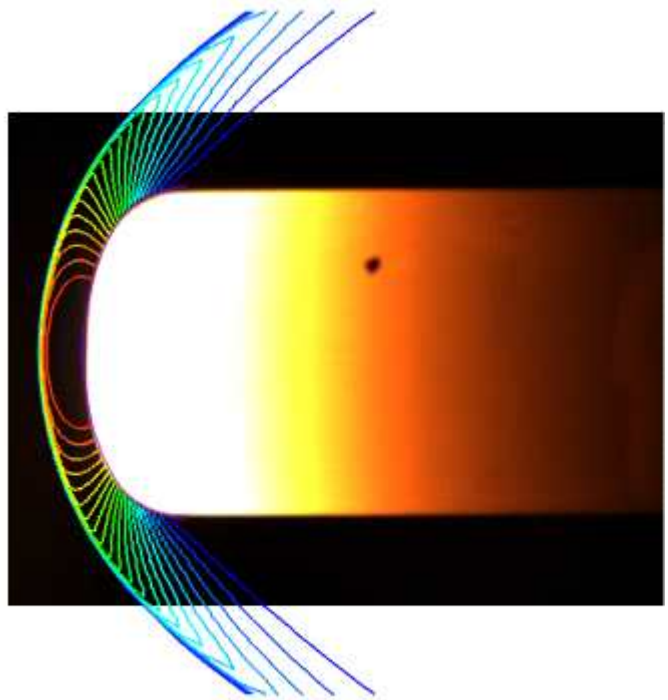

Figure 3.7 Shape change result (No. 1, 60 sec)

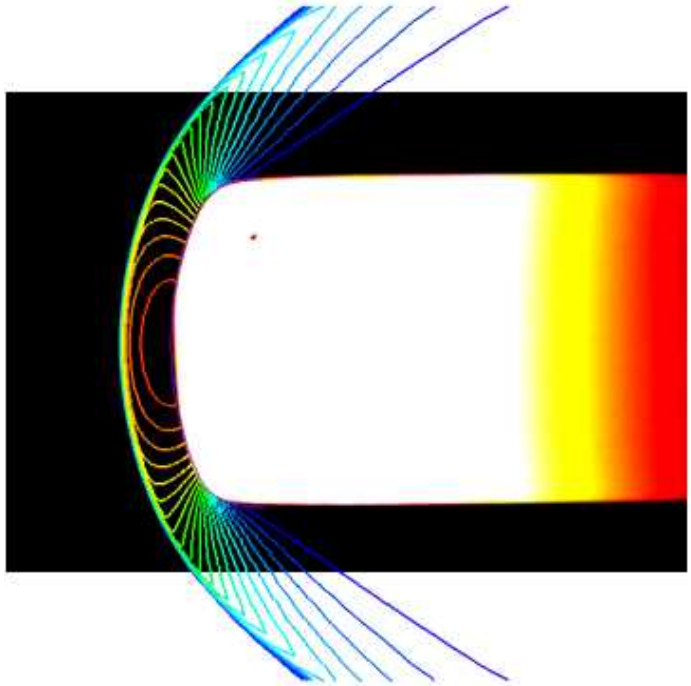

Figure 3.8 Shape change result (No. 2, 60 sec)

3.3 Mass loss analyses with respect to stagnation pressure

3.3.1 Mass loss analyses conditions

Mass loss analyses for the stagnation pressure experiments were carried out using the established ablation analysis framework. The stagnation pressure experiment were carried out for a single flow condition. The freestream flow conditions and species molefraction were calculated and presented in the table. These calculated conditions showed that as the distance increases, the flow further expands making the flow density, pressure, and temperature to decrease and velocity to increase. Also, the expanding flow velocity is large enough so that the species molefraction does not show significant difference with respect to the distance.

Table 3.6 Freestream flow conditions with respect to distance

Distance	Density (kg/m^3)	Velocity (M/s)	Pressure (Pa)	Temp. (K)	Mach number	Enthalpy (MJ/kg)
10mm	8.24E-03	3250	5227	1825	3.4	11.4
20mm	5.30E-03	3355	2868	1556	3.8	11.4
30mm	3.65E-03	3428	1722	1357	4.2	11.4

Table 3.7 Species molefraction with respect to distance

Distance	O	N	NO	O_2	N_2
10mm	3.41E-01	6.31E-03	5.05E-03	7.42E-04	6.47E-01
20mm	3.41E-01	5.93E-03	4.70E-03	7.26E-04	6.48E-01
30mm	3.41E-01	5.72E-03	4.50E-03	7.20E-04	6.48E-01

3.3.2 Mass loss analyses results

Similar to the shape change analyses performed in the previous sub-section, mass loss analyses were performed with the calculated flow conditions and species molefraction. Mass loss analyses were performed for the stagnation pressure experiments. As previously presented in Section 2, the computed results of mass loss and the experimental results of mass loss for the stagnation pressure experiment showed a well-matching result. The well-matching results indicated that the mass loss of pure tungsten due to ablation increases linearly with respect to the stagnation pressure.

4. Tungsten composites' ablation resistance study

Tungsten as a refractory metal has many advantages including high melting point and great mechanical properties. However, there is a crucial disadvantage of tungsten as a refractory metal; weakness to oxidation and ablation when exposed to high-temperature air. In order to overcome these mentioned disadvantages and enhance the high-temperature ablation resistivity, ZrC and HfC carbides were added to pure tungsten to produce tungsten-HfC/ZrC composite. The tungsten composites were manufactured using 3 different methods. Ablation experiments were performed for the manufactured tungsten composites. Ablation characteristics of tungsten composites were evaluated and a number of suggestions to enhance ablation resistivity were made.

4.1 Methods of manufacturing tungsten composites

In order to manufacture tungsten composites, three different methods were used and carbide volume fractions were varied from 10% to 30%.

The first method used to manufacture tungsten composites was named ball-milling method. Tungsten powder and ZrC carbide powder were mixed together using ball-milling. The second method was named high-energy-milling method. Oxide powders(WO_3, ZrO_2) were combined with graphite powder, high-energy milling was then performed to make tungsten-carbide solid solution. The last method is Hybrid method. Hybrid method combines the ball-milling method and high-energy-milling method. Similarly to the high-energy-milling method oxide powders(WO_3, ZrO_2) were combined with graphite powder to produce solid solution, and then ball-milling was used to manufacture tungsten composites. The

overview of the three methods are illustrated below.

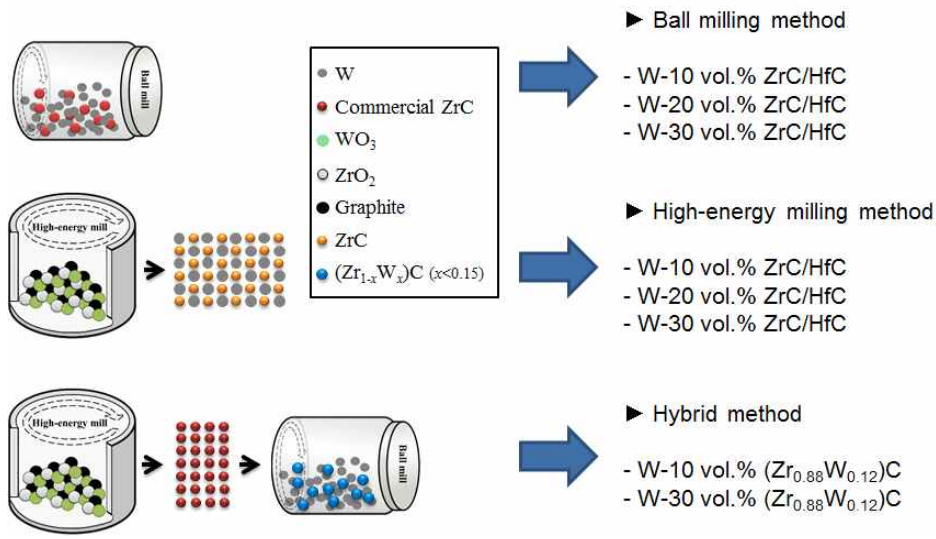

Figure 4.1 Three methods of manufacturing tungsten composites

Micro-structural analyses were performed to study W-ZrC composites' ablation resistivity. The micro-structural analyses results are shown in the below figure. In order to study the ablation resistivity, the composites were post-annealed. The relatively large sized particles for ball-milling method and hybrid method are not well distributed when compared to the particle distribution of high-energy-milling method. Well distributed particles suppress oxygen from spreading which can result in high ablation resistivity.

On the right side of the below figure is the post-annealed micro-structure of the composites. It shows that the particle distributions of composites manufactured using high-energy-milling method does not change much. This indicates that the coherence between the tungsten and ZrC particles are strong.

Micro-structural analyses results of tungsten composites manufactured using different methods suggest that the particle size should be small and

the small particles should be well-distributed to enhance ablation resistance.

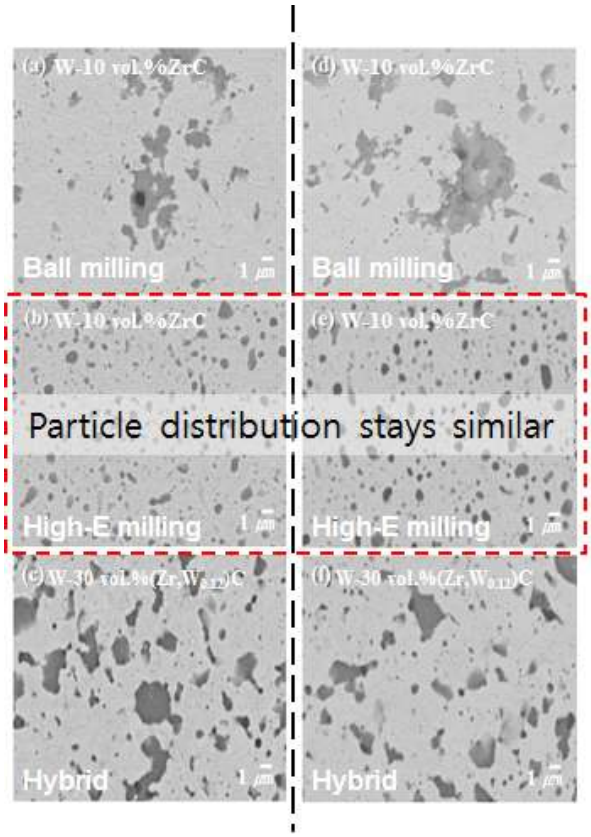

Figure 4.2 Micro-structural analyses results

4.2 Ablation resistivity with respect to HfC fraction

4.2.1 Experimental conditions of W-HfC ablation tests

Ablation experiments were carried out in order to study ablation characteristics and ablation resistivity with respect to the volume fraction of HfC. The volume fraction of HfC were varied; 3, 10, and 20%. The tests were performed changing the exposure time from 5 to 15 seconds with 5 seconds interval. The total number of experiments were 9. The

experimental conditions for these ablation tests were as tabulated in the below table.

Table 4.1 Experimental conditions for W-HfC ablation experiments

No.	Arc current (A)	Flow rate (g/s)	Exposure time (s)	Specimen type
1	360	10	5	W-3vol.%HfC
2			10	
3			15	
4			5	W-10vol.%HfC
5			10	
6			15	
7			5	W-20vol.%HfC
8			10	
9			15	

4.2.2 Experimental results of W-HfC ablation tests

The ablation depth results for W-HfC experiments are as shown below. From the graph in the below figure shows that the amount of recession for the exposure time of 15 seconds varied from about 0.4 to 1.0 mm with respect to the volume fraction of HfC. Similar to pure tungsten, the amount of recession increases as time propagates. And the increase in the volume fraction resulted in decrease in recession depth. The ablation depth of each specimen and that of pure tungsten were compared to calculate increase in ablation resistivity.

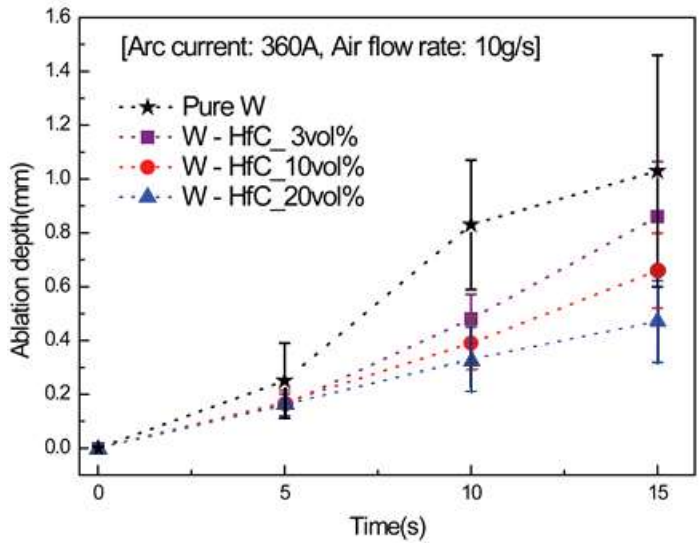

Figure 4.3 Recession amount for each specimen

The below figure illustrates the calculated ablation resistivity increase. It indicates that the ablation resistance of W-HfC increase almost linearly with respect to the volume fraction of HfC up to 20%.

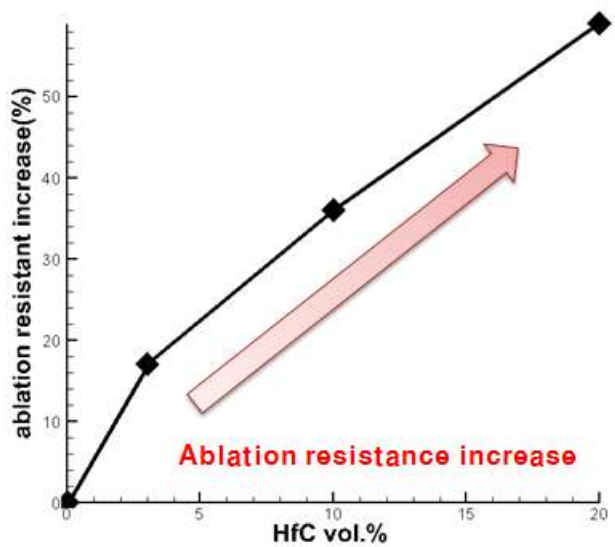

Figure 4.4 Ablation resistance vs vol.%

4.3 Ablation resistivity with respect to ZrC fraction

4.3.1 Experimental conditions of W-ZrC ablation tests

W-ZrC ablation experiments were conducted in addition to W-HfC ablation tests. The volume fraction of ZrC was varied from 10 to 30% with 10% intervals and a few other tests were also conducted. W-10vol%.HfC and W-10vol%.ZrC were compared to study which carbide further increases ablation resistance. In addition, ablation experiments for W-30vol.%(Zr,$W_{0.12}$)C and W-30vol.%(Zr,$W_{0.3}$)C which were manufactured using Hybrid method, were performed to verify the suggestion made earlier in previous sub-section. The total number of experiments were 7 and the test conditions for these are as shown below.

Table 4.2 Experimental conditions for W-ZrC ablation experiments

No.	Arc current (A)	Arc voltage (V)	Exposure time (s)	Specimen type
1	330	10	30	Pure W
2				W-10vol.%HfC
3				W-10vol.%ZrC
4				W-20vol.%ZrC
5				W-30vol.%ZrC
6				W-30vol.%(Zr,W0.12)C
7				W-30vol.%(Zr,W0.3)C

4.3.2 Experimental results of W-ZrC ablation tests

The results in length change of each test were measured and then

compared to that of pure tungsten. The length changes were normalized with respect to the length change of pure tungsten to the increase in ablation resistance. The normalized results are as shown below. It shows that W-10vol.%HfC shows a good ablation resistance compared to the same volume fraction of ZrC, even with a small volume fraction of HfC. W-ZrC composites' ablation resistance increased as the volume fraction increased. When the volume fraction increased from 10 to 20%, it did not show much increase in ablation resistance. However with 30% volume fraction of ZrC, the ablation resistance increased drastically. As for the Hybrid method, ablation resistance decreased by 36%. This was caused by the poor particle distribution which ultimately led to formation of micro-crack on the surface of the specimen. These crack helped oxygen to spread though the specimen which resulted in excessive oxidation. Among the test specimen, 30% voulme fraction W-ZrC showed the most enhanced ablation resistance.

Figure 4.5 Comparison of change in length of each test

4.4 Suggestions to increase ablation resistance

Micro-structural analyses after the ablation tests were performed and the results are shown in below figure. Tungsten and Hf tends to spread towards each other which occasionally forms (W,Hf) metal solution, leading to a greater coherence between small tungsten and hafnium particles. In contrary, tungsten tends to spread towards Zr in W-ZrC composites which makes it hard to form (W,Zr) metal solution, therefore relatively weaker coherence between the particles.

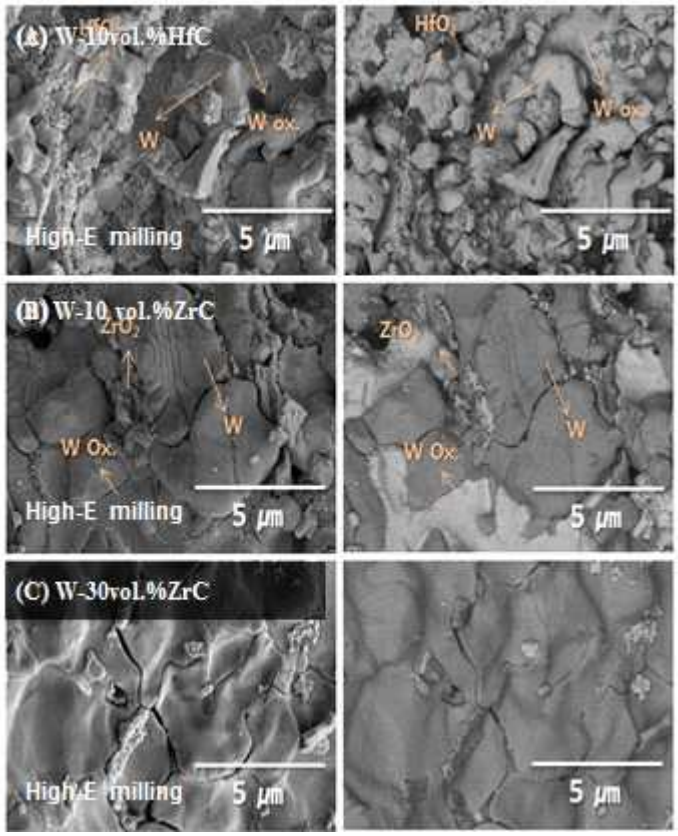

Figure 4.6 Micro-structural analyses results

It can be seen that oxides were formed on the surface of the specimens from the micro-structural analyses results. This oxide layer acts as a type of shield which suppresses the ablation from propagating, ultimately leading to enhanced ablation resistance.

When tungsten particles are in contact with carbide particles, tungsten oxides formed are less likely to be released into surrounding air since the carbide particles suppresses such behavior, from which it can be said that the ablation resistance will increases as the contact surface between tungsten and carbide particles increase. In order to maximize the contact surface, the particles' size has to be small. The effect of particle size on ablation resistance was verified in the previous sections.

In addition, the ablation resistance can be enhanced by forming ZrO_x, or HfO_x layer on the surface. Tungsten oxide (WO_3) has melting temperature of 1746 K and boiling temperature of about 2000 K. These phase change temperatures are relatively low compared to those of HfO_2; melting and boiling temperature of 3031 and 5670 K respectively. Therefore, melting of tungsten oxide is predicted to occur earlier than that of HfO_2. From the CFD analyses results of the pure tungsten experiments, it was shown that the maximum surface temperature reaches the peak value of about 3000 K. The melting point of HfO_2 is even higher than the maximum surface temperature, meaning that melting of HfO_2 is less likely to occur during ablation. In the previous sub-sections, it was suggested that the formation of HfO_x, or ZrO_x can suppress the ablation leading to enhanced ablation resistance. In summary, it is verified from the CFD analyses and micro-structural analyses that the formation of HfO_x, or ZrO_x layer on the surface would enhance the ablation resistance of tungsten composites.

5. Conclusion

In this study, ablation experiment for pure tungsten and tungsten composites were performed with addition of CFD analyses.

Ablation characteristics of pure tungsten that the amount of ablation increases as enthalpy increases and the amount of recession increases linearly with respect to stagnation pressure was seen from the enthalpy changing experiments and the stagnation pressure changing experiments for pure tungsten specimens.

Ablation phenomenon analysis framework was established to overcome the limitations of ablation experiments. Using the established analysis framework, it was possible to predict how ablation in tungsten would propagate from the input parameters of the plasma generator. Also, many additional values such as surface and interior temperature distribution which were then used in further research became obtainable.

In order to overcome the crucial disadvantages of tungsten; weakness to oxidation and ablation in high-temperature flow, W-ZrC, and W-HfC composites were manufactured using 3 different methods. Micro-structural analyses and ablation tests were conducted for the tungsten composites in order to study the ablation characteristics and ablation resistance of the composites. It was seen that the ablation resistance increased as the volume fraction of ZrC and HfC increased. Additionally, it was suggested that the formation of small particles through the specimen and ZrO_x, HfO_x layer on the surface of the specimen could increase the ablation resistance.

6. References

[1] 김원영, (1991), “ZrCl4-Mg-C 계 반응에 의한 탄화지르코늄 분체(ZrC)의 합성”, 요업학회지 , 28, 4

[2] 박홍채, 이윤복(1994), “지르콘의 탄소열환원에 의한 ZrC/SiC의 합성”, 공업화학, 5, 6

[3] 유영수, 조창용. (2004), “극한 환경용 내열재료 기술 현황 분석”, 한국 기계 연구원.

[4] 이형복, (1995), “SHS법에 의한 ZrC 합성 및 온도 Profile 분석”, 요업학회지, 32, 6

[5] 정진기. (2001): “주요광물 소재의 개발동행 분석”, 기초기반사업 최종 보고 연구서

[6] 최국선, (2007), “진공융해법에 의한 고순도 희유금속 제조 및 평가 기술 개발”, 한국지질자원연구원

[7] Barraud, E. (2008), “Mechanically activated solid-state synthesis of hafnium carbide and hafnium nitride nanoparticles” J. of Alloys and Compounds, 456, 224-233.

[8] E. WUCHINA., (2004), “Designing for ultrahigh-temperature applications: the mechanical and thermal properties of HfB2, HfCx, HfNx, and α Hf(N)”, J. of Materials Science, 39, 5939-5949.

[9] Fertig M., Fruhauf H. H., (1999), “Detailed Computation of the Aerothermodynamic Loads of the MIRKA Capsule“, Proceedings of the 3rd European Symposium on Aerothermodynamics for Space Vehicles, ESA SP-426.

[10] Garkusha, I. E. et al. (2009), “Experimental study of plasma energy transfer and material erosion under ELM like heat loads“, Journal of nuclear materials, 390-391, 814-817.

[11] Garkusha, I. E. et al. (2009), “Damage to preheated tungsten targets after multiple plasma impacts simulating ITER ELMs“, Journal of nuclear materials, 386-388, 127-131.

[12] Gordon, S. and McBride, B. J. (1994), “Computer Program for

Calculation of Complex Chemical Equilibrium Compositions and Applications“, I.Analysis, NASA Reference Publication 1311.
[13] Gui-Ming Song, (2003), “Thermomechanical properties of TiC particle-reinforced tungsten composites for high temperature applications”, Int. J. of Refractory Metals & Hard Materials, 21, 1-12
[14] Gupta, R. N., Yos, J. M., Thompson, R. A., Lee, K. P. (1990), “A Review of Reaction Rates and Thermodynamic and Transport Properties for an 11-Species Air Model for Chemical and Thermal Nonequilibrium Calculations to 30000 K“, Technical Report, NASA RP-1232.
[15] Jiecai Han, Ping Hu, Xing-Hong Zhang, Songhe Meng, (2007), “Oxidation behavior of zirconium diboride–silicon carbide at 1800 ° C”, Scripta Materialia, 57 [9], 825-828.
[16] M. Liu & J. Cowley (1992), “Hafnium carbide growth behavior and its relationship to the dispersion hardening in tungsten at high temperatures”, Material Science and Engineering, A160, 159-167
[17] Lee, J. I., (2007), “A Study on Numerical Modeling for Flow Analysis in Arc-Heaters,” Phd thesis, Seoul National University.
[18] M. Rosso. (2006): “Ceramic and metal matrix composites: Routes and properties”, J. of Materials Processing Technology 175, 364-375.
[19] Murphy, A. B. (1995), “Transport Coefficients of Air, Argon-Air, Nitrogen-Air, and Oxygen-Air Plasmas,” Plasma Chem. Plasma Process. Vol. 15, No. 2, pp. 279-305.
[20] Michael D. (2004): “Carbothermal reduction synthesis of nanocrystalline zirconium carbide and hafnium carbide powders using solution-derived precursors”, J. of Materials Science 39 6057–6066,
[21] Mickael Dolle (2007): “Synthesis of nanosized zirconium carbide by a sol–gel route”, J. of the european ceramic society 27 2061–2067
[22] Park, C. (1990), “Non-equilibrium Hypersonic Aerothermodynamics“, Willey-Interscience, John Wiley and Sons, Inc., New York.
[23] Park, C. (2001), “Chemical-Kinetic Parameters of Hyperbolic Earth Entry,” Journal of Thermophysics and Heat Transfer, Vol. 15, No. 1,

pp. 76 ~ 90.
[24] Qingfeng Tong et al., (2004), “Resistance to ablation of pitch-derived ZrC/C composites“, Carbon, 42, 2495-2500.
[25] Sakai, T. and Olejniczak, J. (2003), “Improvement in a Navier-Stokes Code for Arc Heater Flows,” AIAA Paper 2003-3782.
[26] Savino R. et al., (2008), “Arc-jet testing on HfB2 and HfC-based ultra-high temperature ceramic materials“, Journal of the european ceramic society, 28, 1899-1907.
[27] Schreiber, P. W., Hunter II, A. M., and Benedetto, K. R. (1973), “Electrical Conductivity and Total Emission Coefficient of Air Plasma,” AIAA Journal, Vol. 11, pp. 815-821.
[28] Sufang Tang et al., (2007), “Ablation behaviors of ultra-high temperature ceramic composites“, Materials Science and Engineering A, 465, 1-7.
[29] Zhang. (2008): “Compressive deformation behavior of a 30 vol.%ZrCp/W composite at temperatures of 1300-1600 ° C”, Materials Science and Engineering A 474 382-389,
[30] Zhang (2008): “Effect of particle clustering on the effective modulus of ZrC/W composites”, International J. of refractory metal & hard materials 27 14-19
[31] Song, G.-M., et al. (2003). “Effect of carbide particles on the ablation properties of tungsten composites.“ Materials characterization 50(4): 293-303.
[32] Chiang, T. L., et al. (1993). “Analysis of nosetip recession of the tungsten projectiles in hypersonic flight. “
[33] Dickerson, M., et al. (2004). “Near net-shape, ultra-high melting, recession-resistant ZrC/W-based rocket nozzle liners via the displacive compensation of porosity (DCP) method.“ Journal of Materials Science 39(19): 6005-6015.
[34] Jung, I.-J., et al. (1999). “A study of the formation of Ti (CN) solid solutions.“ Acta materialia 47(11): 3241-3245.

[35] Winovich, W. (1964). “On the equilibrium sonic-flow method for evaluating electric-arc air-heater performance.”, National Aeronautics and Space Administration.
[36] Kartono, R. (2007). “Effects of Platinum, Iridium, and Hafnium to Nickel-Aluminium Alloys under Cyclic Oxidation Conditions.”, The University of New South Wales Australia.
[37] Gaskell, D. R. (2008). Introduction to the Thermodynamics of Materials: CD-ROM, Taylor & Francis US.

국문초록

로켓 노즐용 고강도 내열금속 소재의 삭마 현상에 대한 연구

Pyungkee kim
School of Mechanical and Aerospace Engineering
The Graduate School
Seoul National University

순수 텅스텐과 W-HfC, W-ZrC 복합재에 대한 삭마 실험 및 CFD를 이용한 전산해석을 통하여 이들의 삭마 특성과 내삭마/산화성에 대한 연구를 수행하였다. 엔탈피와 정체 압력에 대한 순수 텅스텐의 삭마 특성을 파악하기 위하여 여러 종류의 실험을 수행하였으며, 삭마 깊이는 엔탈피가 증가함에 따라 증가하는 경향을 나타내었고, 질량 삭마량은 정체 압력에 선형적으로 비례하는 것을 확인하였다. 이에 추가적으로 텅스텐 삭마 현상 전산해석 통합 framework를 정립하였다. 정립된 framework를 통하여 순수 텅스텐을 대상으로 수행한 실험에 대한 전산해석을 하였으며 이로부터 실험으로는 측정할 수 없었던 유동 조건 및 삭마 현상으로 인한 텅스텐 시편의 변화, 최대 표면 온도 및 시편 내부 온도 분포를 계산하였다. 또한, 순수 텅스텐의 약점 중 하나인 고온의 공기에 대한 산화/삭마 취약성을 보완하기 위하여 3 가지 방법을 이용하여 W-ZrC, W-HfC 복합재를 제작하였다. 제작된 복합재를 대상으로 삭마 실험과 미세구조 분석을 수행하였으며 이로부터 텅스텐 복합재의 제작 방식과 강화재 함량에 대한 삭마 특성

및 내삭마/산화성 변화에 대한 연구를 수행하였다. 위와 같은 삭마 실험, 전산해석, 미세구조 분석 연구의 결과로 W-ZrC, W-HfC 텅스텐 복합재의 내삭마/산화성을 향상시킬 수 있는 방안을 제시하였다. 제시된 W-ZrC, W-HfC 복합재의 내삭마/산화성 향상 방안은 첫째로 텅스텐 및 탄화물 입자의 크기가 작게 제작하는 것과, 둘째로 표면에 ZrOx, HfOx 층을 형성하여 삭마/산화를 억제하는 방안이 제시되었다.

주요어 : 삭마, 텅스텐, W-HfC, W-ZrC, 내삭마성, CFD

학 번 : 2013 - 20662